



HAL
open science

Modelling propagation of sinkhole, in both slow and dynamic modes, using the UDEC computer code

Attalah Abbass Fayad, Marwan Al Heib, Christophe Didier

► To cite this version:

Attalah Abbass Fayad, Marwan Al Heib, Christophe Didier. Modelling propagation of sinkhole, in both slow and dynamic modes, using the UDEC computer code. 5. North American Rock Mechanics Symposium & 17. Tunneling Association of Canada Conference, Jul 2002, Toronto, Canada. pp.695-703. ineris-00972371

HAL Id: ineris-00972371

<https://ineris.hal.science/ineris-00972371>

Submitted on 3 Apr 2014

HAL is a multi-disciplinary open access archive for the deposit and dissemination of scientific research documents, whether they are published or not. The documents may come from teaching and research institutions in France or abroad, or from public or private research centers.

L'archive ouverte pluridisciplinaire **HAL**, est destinée au dépôt et à la diffusion de documents scientifiques de niveau recherche, publiés ou non, émanant des établissements d'enseignement et de recherche français ou étrangers, des laboratoires publics ou privés.

Modelling propagation of sinkhole, in both slow and dynamic modes, using the UDEC computer code.

(Methodology and application)

ABBASS FAYAD Atallah* : E-mail : aafayad@mines.u-nancy.fr

AL HEIB Marwan* : E-mail : Heib@mines.u-nancy.fr

DIDIER Christophe** : E-mail : Christophe.Didier@ineris.fr

LAEGO (Laboratoire Environnement, Géomécanique et Ouvrages) – INERIS (Institut National de l'Environnement industriel et des RISques) :

Adresse* : Ecole des mines de Nancy, Parc de Saurupt, 54042 Nancy-Cedex, France ;

Adresse** : Verneuil-en-Hallate PO Box. No.2 65, France ;

Tel. : 0033 3 83 58 42 89 ; Fax : 0033 3 83 53 38 49.

ABSTRACT:

The propagation of sinkhole phenomena towards the surface is a fairly complex phenomenon, with the potential to cause damage to surface structures within the affected area. Using numerical modelling a methodology has been developed which makes it possible more closely to specify the conditions in which sinkhole forms and to propose a prediction model. The UDEC code is used. An actual case of sinkhole in the Paris region (Vachat, 1982) has been used as a basis for the study. We simulated the predicted collapse mechanism and the profile of the sinkhole itself. The influence of a surface structure was also examined. The modelling process in static and dynamic modes was developed in order to simulate the ways in which sinkhole forms. As regards dynamic modelling, we determine the relevant parameters: critical damping and fundamental frequency. The dominant point in this method is that induced fractures in the roof strata overlying underground excavations – the root cause of sinkhole – are created by hand. The fractures were induced using the criterion whereby a zone is formed in which the failure criterion is exceeded. The comparison between observation and the modelling results is very satisfactory. It may be noted that the numerical modelling and the methodology used enabled us to determine the shape and parameters of the roof “bell” and of the zone of sinkhole. We were also able to confirm the influence of external loads that might facilitate development of the sinkhole. A feature of dynamic (rapid) appearance of sinkhole is apparently that it takes place on a bigger scale. Incidentally such an approach could be used to examine the consequences for structures.

Keywords: Sinkhole, structure, propagation, influence, modelling, static calculation, dynamic calculation, forecasting methodology.

1. INTRODUCTION

When ground - frequently stratified - collapses owing to the presence of underground voids, particularly in shallow mines and quarries, the phenomenon propagates upwards in a bell-shaped profile and can induce sinkhole at the surface (fig. 1). Underground the bell-shaped profile is usually characterised by its height (h), its diameter (D) and an angle that serves to indicate the shape of the bell (α). At the surface, sinkhole is characterised by its depth (P) and diameter (ϕ).

Observations of different cases of sinkhole have been used to propose empirical prediction equations (Vachat, 1982). Although pragmatic, this approach is not accurate enough and is limited to areas that are geologically uniform and hence fairly limited in extent. Approaches based upon the strength of materials are often used for these predictions (Didier et Tritzsch, 1996).

These types of sinkhole are frequently the cause of more or less substantial damage depending on their dimensions and on the type of structure (fig. 1). Any attempt to

improve the behaviour of structures, once sinkhole has appeared, is a tricky business.

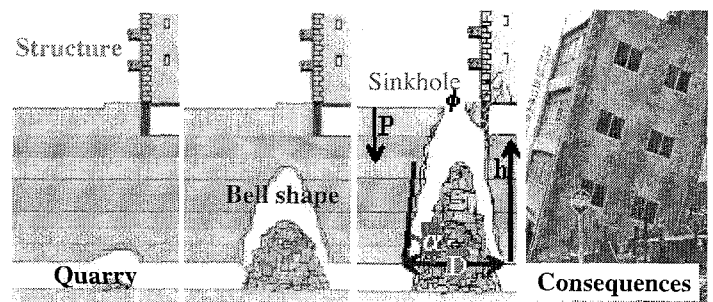


Figure 1 : Development of sinkhole and induced consequences.

This article seeks to improve the prediction of sinkhole development and its consequences for structures (fig. 1) using modern methods (numerical modelling using distinct elements, UDEC). This new approach makes it possible to determine the probable profile of the sinkhole and to specify the influence of structures according to the behaviour of the ground.

2. CHOICE OF PROGRAM AND METHODOLOGY

The failure mechanism involved in sinkhole, in the case of stratified rock, is the yielding of the different roof strata (Peng et al, 1981). It is possible, using the finite element method in the UDEC code (Itasca), to localise the failure zones where the criterion is exceeded.

On the other hand it is not possible with UDEC to create induced fractures within these zones. For simulating the failure of the strata, the possible fall of blocks, and the appearance of sinkhole at the surface, we propose to generate these fractures by hand.

We assumed that rock failure was likely to occur when plasticity developed along the cross-section of a given block. On the other hand if the areas of plasticity are discontinuous, we shall speak of partial failure (partial fracturing), and the block concerned is regarded as not undergoing any geometrical change. This is a progressive approach: we begin the process with the first block in the roof and then apply it to the others. The analysis terminates when no more new fractures can be created using the above criterion.

3. DESCRIPTION OF THE CASE INVESTIGATED

3.1. Description of the site and properties

For the purposes of this methodological study, we turned to an actual case of sinkhole in the Paris region. The quarry involved was shallow (8 m) and had been excavated using the room and pillar method. The depth of the block worked did not exceed 2 m, giving a ratio of overburden to gallery height of less than four. The sinkhole had a diameter of 2.5 m and a depth of 2 m (Vachat, 1982). The bell profile formed was characterised by an angle of 80° at the base. The overburden consisted of a series of blocks of limestone, marl and clay.

3.2. Simulating the case using UDEC

The aim is to produce a model to simulate the development of sinkhole. Sinkhole usually has a conical profile. The model adopted in two dimensions is based upon the assumption of plane deformations. This assumption is more pessimistic than that of axial symmetry (not available in UDEC), a fact confirmed by Mandel (1966) who compared the two solutions for a cylinder and a sphere. The equations for the stresses (σ_θ and σ_r) given below are for a semi-infinite cylinder of radius (a):

$$\sigma_{r \text{ tunnel}} = \sigma_0(1-a^2/r^2), \quad (1)$$

$$\sigma_{\theta \text{ tunnel}} = \sigma_0(1+a^2/r^2). \quad (2)$$

The equations for the distribution of the stresses (σ_θ and σ_r) around a sphere of radius (a) that represents the model with symmetry of revolution are:

$$\sigma_{r \text{ sphere}} = \sigma_0(1-a^3/r^3), \quad (3)$$

$$\sigma_{\theta \text{ sphere}} = \sigma_0(1+a^3/2r^3). \quad (4)$$

Figure 2 shows a comparison of the solutions for the two approaches. It can be seen that the difference is significant, particularly at a distance of one to two times the radius of the cavity

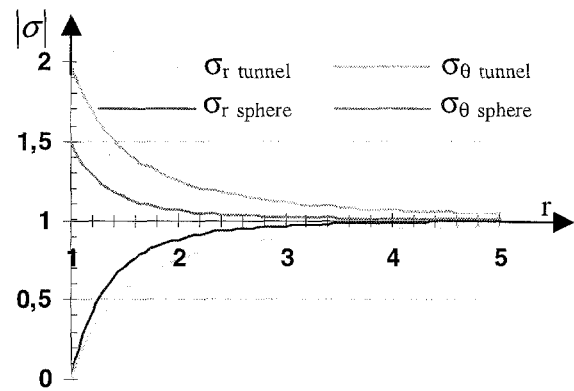


Figure 2 : Distribution of stresses, for $a = 1\text{m}$ and $\sigma_0 = -1\text{Mpa}$.

3.3. Law governing the behaviour of materials

The model is elastic-plastic with behaviour of the softening type (negative work-hardening). This represents the behaviour of the rock under stresses that are induced in the vicinity of the underground workings (Piguet 1983 and Fine 1993).

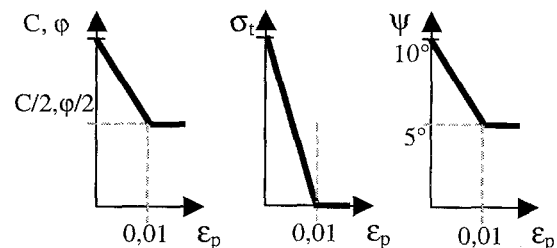


Figure 3 : Relations between C , φ , σ_t , ψ and ϵ_p .

In the plastic zone, the work-hardening variable depends on the plastic distortion (Prévost and Hoeg, 1975). The variation in cohesion (C), the angle of friction (φ), the tensile strength (σ_t), and expansion (ψ) as a function of the plastic deformation (ϵ_p), are shown on figure 3. In certain cases, the initial values of C and φ fall by half with the value σ_r falling to zero, for a value of plastic deformation (ϵ_p) of 1% (Tharp, 1995). These factors are taken into account in our study.

3.4. Law governing the behaviour of junctions

Force-displacement equations are used in UDEC to indicate the behaviour of junctions. We used an elastic-plastic law with variable stiffness (a function of the stress normal to the junction plane σ_n , $jK = a\sigma_n^b$). The values of (a) and (b) are functions of the stiffness (normal or tangential) respectively. They are given by the following equations:

$$jK_n = 100\sigma_n^2, \quad (5); \quad jK_s = 10\sigma_n^2. \quad (6)$$

Figure 4 shows the model adopted. Table 1 shows the different roof blocks used in the model, from the top to the bottom of the gallery. Their mechanical properties

were taken from the literature relative to the Paris basin (Filliat 1984), with:

e : thickness of the block concerned; ρ : the density;

ν : Poisson's coefficient; E : Young's modulus.

The values of normal and tangential stiffness (K and G) for the materials were deduced from the following expressions:

$$K = E/3(1-2\nu), \quad (7) \quad G = E/2(1+\nu). \quad (8)$$

| Mat | e (m) | ρ T/m ³ | ν | E MPa | σ_t MPa | C MPa | ϕ (°) | K MPa | G MPa |
|-----|---------|-------------------------|-------|---------|----------------|---------|------------|---------|---------|
| 6 | 1.0 | 2.2 | .25 | 50 | 0.1 | 0.2 | 26 | 30 | 20 |
| 7 | 1.0 | 2.2 | .25 | 50 | 0.2 | 0.4 | 27 | 30 | 30 |
| 3 | 0.5 | 2.2 | .25 | 130 | 0.2 | 1.2 | 30 | 80 | 60 |
| 2 | 0.5 | 2.2 | .25 | 100 | 0.3 | 0.8 | 29 | 60 | 50 |
| 1 | 1.2 | 2.2 | .25 | 70 | 0.3 | 0.8 | 28 | 40 | 30 |
| 2 | 0.8 | 2.2 | .25 | 100 | 0.3 | 0.8 | 29 | 60 | 50 |
| 1 | 1.0 | 2.2 | .25 | 70 | 0.3 | 0.8 | 28 | 40 | 30 |
| 3 | 1.25 | 2.2 | .25 | 130 | 0.2 | 1.2 | 30 | 80 | 60 |
| 4 | 2.0 | 2.2 | .25 | 250 | 0.8 | 2.0 | 31 | 150 | 100 |
| 5 | 5.0 | 2.2 | .25 | 850 | 10 | 10 | 35 | 500 | 500 |

Table 1: Mechanical and geometrical properties of materials.

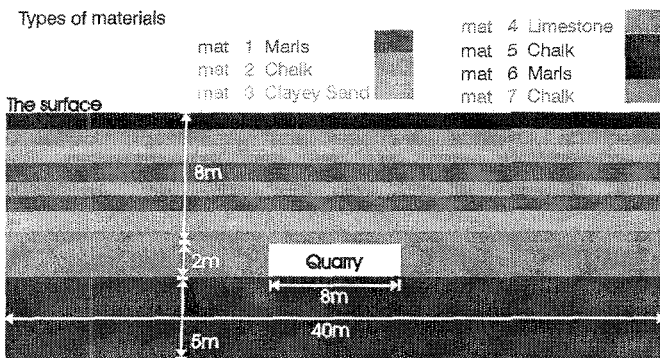


Figure 4: Cross-section and materials in UDEC.

The properties of the junctions between strata are shown in table 2. The maximum and minimum values of normal ($\max jK_n$ and $\min jK_n$) and tangential ($\max jK_s$ and $\min jK_s$) stiffnesses are functions of the values of K and G for the corresponding materials (based upon experience).

| Junction No | 1 | 2 | 3 | 4 |
|-------------------|-----|-----|-----|-----|
| $\max jK_n$ (Mpa) | 30 | 40 | 60 | 80 |
| $\max jK_s$ (Mpa) | 15 | 20 | 30 | 40 |
| $\min jK_n$ (Mpa) | 20 | 30 | 50 | 60 |
| $\min jK_s$ (Mpa) | 10 | 10 | 30 | 30 |
| $j\phi$ (°) | 20 | 20 | 20 | 22 |
| $j\sigma_t$ (MPa) | 1 | 1 | 1 | 1 |
| jC (MPa) | 100 | 100 | 100 | 100 |
| ψ (°) | 10 | 10 | 10 | 10 |

Table 2: Mechanical properties of junctions.

It is recalled that the angle of friction of the junctions ($j\phi$) were obtained by Filliat (1984) and Fine (1993). We also assumed that the simple tensile strength ($j\sigma_t$) was zero, cohesion (jC) negligible, and the angle of expansion of the junctions as given in the UDEC manual (Itasca, 1996).

For the purposes of this modelling process, it is necessary to estimate the tensor of the initial stresses (no measured data are available). We assumed that the ground was subjected to its own weight and therefore to a vertical stress of $\rho\gamma h$ and a horizontal stress of $0.3 \rho\gamma h$.

3.5. Results of the simulation (formation of sinkhole)

Figure 5 represents the potential zones of failure following simulation of the excavation of the gallery. It can be seen that the first block is liable to fracture in two zones. These failure zones are replaced by two fractures forming a central block and two parts that appear to overhang (figure 6).

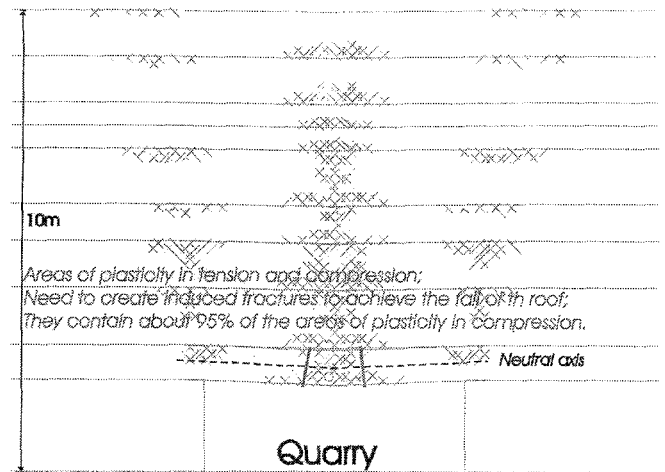


Figure 5: Location and creation of induced fractures.

Figure 6 shows the configuration obtained, which will be modelled in its turn. This simulation is one of the intermediate stages moving towards final equilibrium. After creating these fractures, a new stage of calculation is undertaken with a further analysis of the zones of plasticity in this intermediate stage.

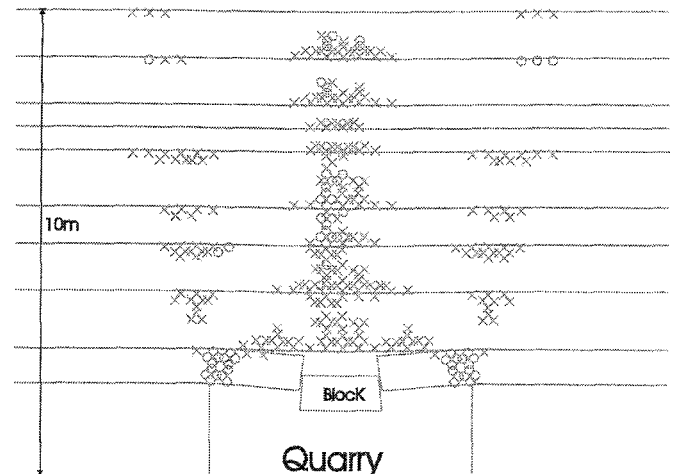


Figure 6: Intermediate phase of creating induced fractures.

The presence of new zones means that the creation of new fractures is repeated up to equilibrium and the complete stability of the roof with or without the appearance of sinkhole at the surface (fig. 7).

Figure 8 shows the final shape of the cavity after the seven phases of calculations. Equilibrium has been reached following the failure of the 7th block (fig. 8). It will be

noted that the failure zones cannot generate further blocks. **In conclusion, no sinkhole has reached the surface.**

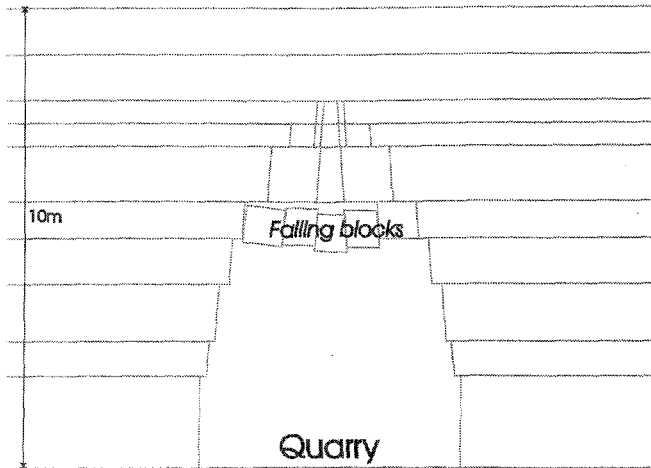


Figure 7: Intermediate phase of the final calculation.

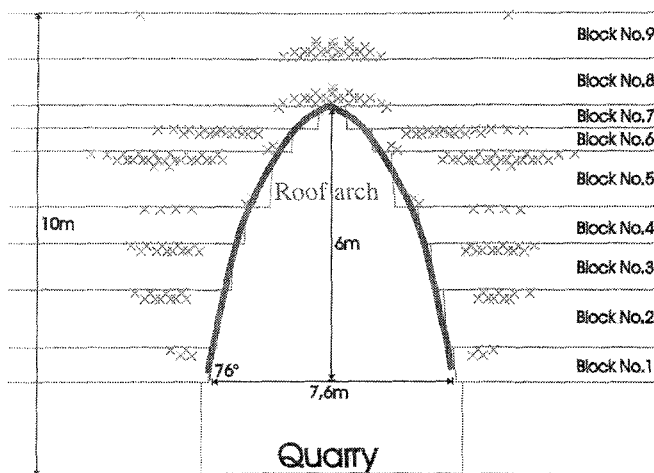


Figure 8: Final configuration for the case examined.

In this configuration, the bell shape is characterised by a height (h) of 6 m, a base angle (α) of 76° and a diameter at the base (D) of 7.6 m.

Table 3 shows the lengths of different blocks in the roof. It can be seen that the span of the blocks diminishes as we approach the surface.

| Block No. | Block depth (m) | Length of failed span (m) |
|-----------|-----------------|---------------------------|
| 1 | 7.25 | 7.60 |
| 2 | 6.00 | 7.10 |
| 3 | 5.00 | 6.20 |
| 4 | 4.20 | 5.40 |
| 5 | 3.00 | 3.84 |
| 6 | 2.50 | 2.50 |
| 7 | 2.00 | 1.00 |
| 8 | 1.00 | 0.00 |
| 9 | 0.00 | 0.00 |

Table 3: Lengths of failed spans.

3.6. Simulation of a surface structure in the model

To examine the influence of aggravating factors on the speed of propagation of the sinkhole to the surface, and on the resulting consequences for the structures affected,

we simulated the presence of a four-storey building above the underground cavity.

Figure 9 shows a plan view of one floor of the building with the data necessary for calculating the loads acting on the pillars P_1 , P_2 and P_3 . The transverse section (X-X) shows the loads transmitted to the ground at the foundations (A, B and C). The transmitted loads are calculated in a simplified manner. The results show a load of 100 kN under the foundations A and C and a load of 200 kN under the foundation B.

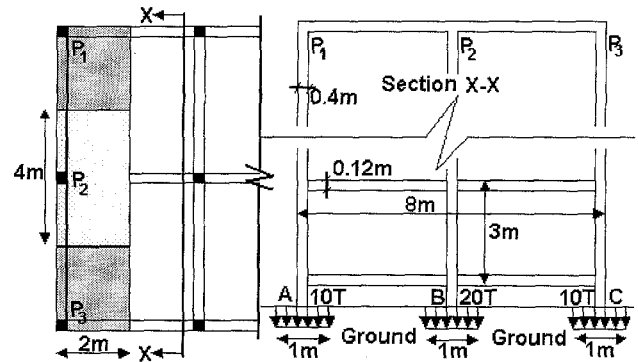


Figure 9: Illustration of the simulated building.

Owing to the difficulty of simulating structures in UDEC, the load of the structure is simulated by applying normal stresses, like boundary conditions, equivalent to the loads calculated in the previous paragraph. These are placed (fig. 10) respectively above the centre of the gallery (100 kN), above the right-hand boundary (200 kN) and 4 m from the right-hand boundary (100 kN), each 1 metre wide.

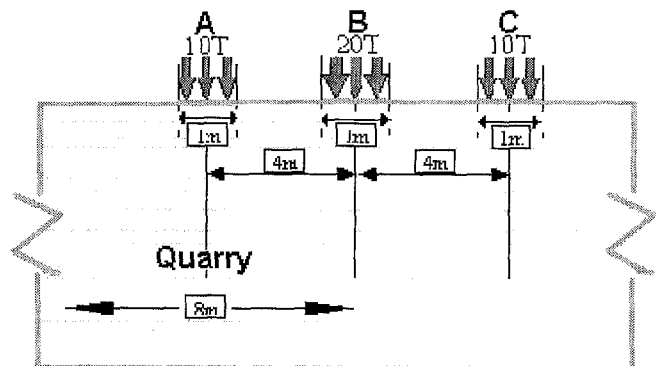


Figure 10: Incorporating the building in UDEC.

3.7. Analysis of the final configuration

The procedures indicated earlier are applied to the new model, to establish the same criterion for generating fractures. Figure 11 shows the configuration of the sinkhole. This is generated beneath foundation A in the centre of the model.

The bell-shaped sinkhole formed is characterised by: a height (h) of 8 m, a base angle (α) of 76° and a diameter at the base (D) of 7.6 m. The form of the sinkhole is characterised by a diameter at the surface (ϕ) under foundation (A) of 1.5 m. The mean lengths of fractured spans in the roof blocks (with structure) are shown in table 4, from the bottom up.

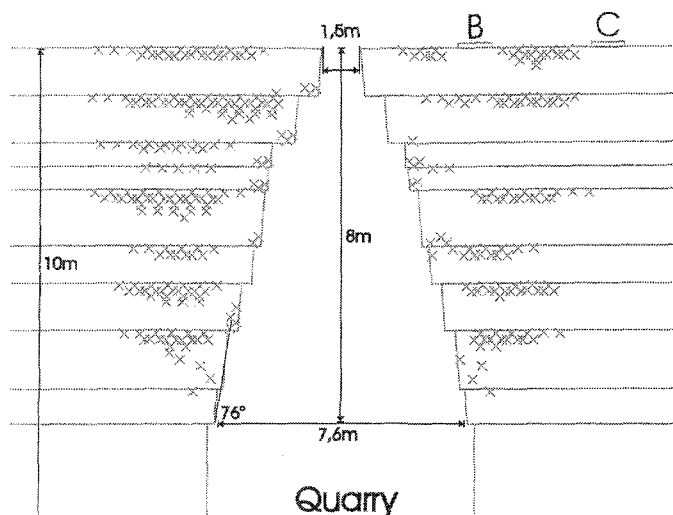


Figure 11: Final configuration with structure.

| Block No. | Block depth (m) | Length of failed span (m) |
|-----------|-----------------|---------------------------|
| 1 | 7.25 | 7.60 |
| 2 | 6.00 | 7.10 |
| 3 | 5.00 | 6.20 |
| 4 | 4.20 | 5.40 |
| 5 | 3.00 | 4.84 |
| 6 | 2.50 | 4.30 |
| 7 | 2.00 | 4.10 |
| 8 | 1.00 | 2.80 |
| 9 | 0.00 | 1.50 |

Table 4: Lengths of failed spans (with structure).

Comparison of tables 3 and 4 shows that the blocks of depth greater than 3m are unaffected by the presence of the building. The lengths of the failed spans are the same in the two models. This may be explained by the width of the foundations ($l = 1$ m), and the influence of the loads does not exceed a depth of 3 times l ($= 3$ m in the particular case examined). For the other blocks however, the influence of the building shows up clearly as an increase in the length of the failed spans and by the occurrence of sinkhole (fig. 11).

4. SIMULATION IN DYNAMIC MODE

The aim of this simulation is to investigate the rapid formation of sinkhole. We assumed that there is not sufficient time for the rock mass to damp out the shocks induced by the failure of the roof blocks. This type of calculation requires data such as the fundamental frequency (f_p) of the model and its critical damping (ξ_c).

4.1. Sizing the dynamic model and the calculation mesh

In order to meet the requirements of the dynamic mode calculation, the model has to be resized: the dynamic calculation is affected to a greater extent by the size of the model and that of the mesh (due to wave reflection). Figure 12 shows the cross-section of the model together with the proposed mesh (table 5) which will be validated numerically after calculating f_p .

For the dynamic mode calculation to be reliable, the maximum size (T) of the zones (or elements) should not exceed approximately $1/8$ of the wavelength (λ) to be

transmitted which has the highest frequency (f_{max} , Pecker 1984, Cundall 1980): $T \leq \lambda/8 = 1/8 * C/f_{max}$ (10). C is being the wave propagation speed.

| Y (depth) | Mesh size |
|-----------------------|-----------|
| Between 0 and 10 m | 0,5m |
| Between -10 and 0 m | 1,0m |
| Between -20 and -10 m | 3,0m |
| Between -50 and -20 m | 5,0m |

Table 5: Variation in mesh size with depth.

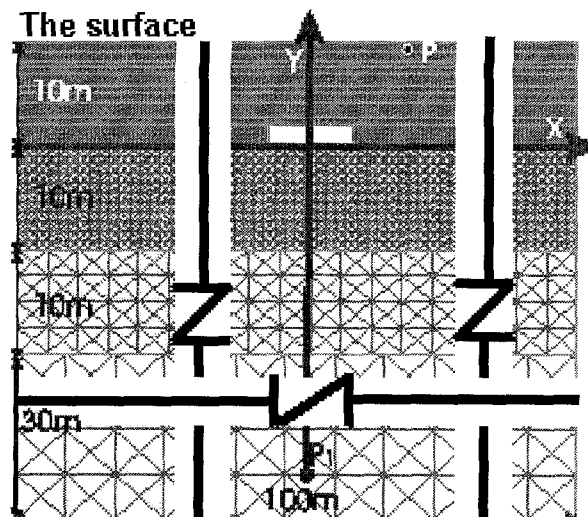


Figure 12: Cross-section and mesh used for dynamic calculation.

4.2. Calculation of critical damping (ξ_c)

The value of critical damping can be selected from experimental values found in the literature. The value taken was between 2.5 and 5%. For $f_p < 10$ Hz, it is necessary to multiply ξ_c by two (El-Shabrawy 1996).

4.3. Calculation of the fundamental frequency (f_p)

Calculating the value of f_p involves looking for the fundamental frequency of the system (the lowest frequency). To do this, we carried out a calculation without damping by applying only static loading, and then recorded the system response (speed or displacement) at any point (fig. 13). Since there is no damping, the system oscillates freely and its fundamental frequency can be determined from observation of its oscillations (El-Shabrawy, 1996).

Zero damping should always be introduced after simulating the excavation, however one may wonder whether this phenomenon takes place before or after static equilibrium. The dynamic effects of an earthquake are often introduced after static equilibrium. In our case, zero damping is applied with respect to two options: the excavation carried out without induced fractures (fig. 5) and the second after formation of the bell shape (fig. 8).

Calculation of f_p was done at two points in the model P (10; 9.5) and P1(0; -45) as shown in figure 12. The point P is placed above the gallery in order to optimise f_p in the zone of high perturbation. P1 however is placed at the bottom of the model in order to optimise f_p in the zone of low perturbation. Figure 13 shows how the velocity varies as a function of time at the points P and P1 for zero damping. The two figures (13-a) and (13-b) are obtained for the first option. The resulting values for f_p are 17 and

20 Hz respectively. The two figures (13-c and 13-d) correspond to the second option. The result is values of f_p of 4 and 10 Hz respectively. We can see therefore that f_p varies between 4 and 20 Hz (fig. 13). This variation is due to the method of applying zero damping and to the behaviour of each stratum (block), particularly in the zones that are affected or perturbed by the excavation.

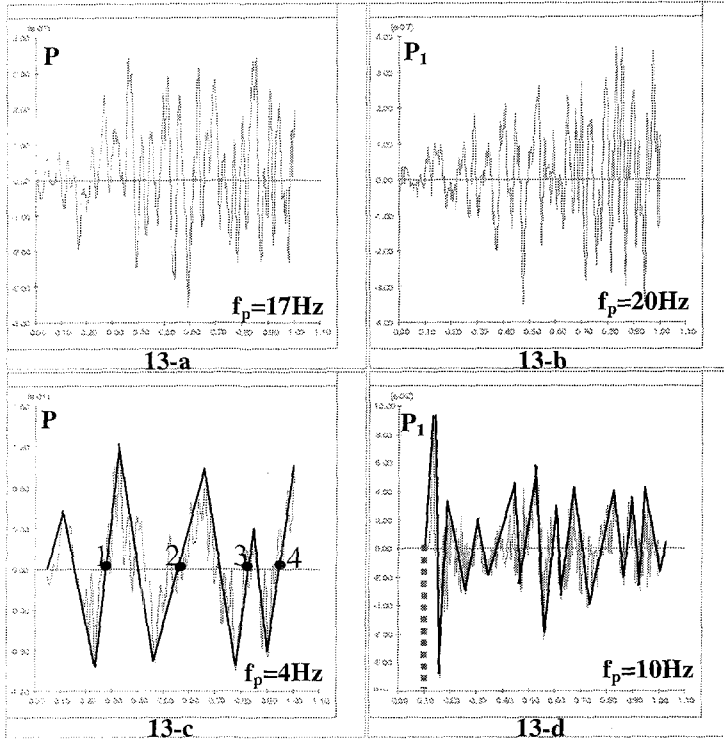


Figure 13: Calculation of f_p using the method of $\xi_c = 0$.

The mesh used is in fact verified for the minimum velocity. From figure 13 it can be seen that the minimum velocity of the wave is that of figure 13-d). The time the wave takes to reach the point P_1 is 0.1s. The distance between the origin of the frame of reference (fig. 12) and P_1 is easily calculated ($d = 45$ m). We conclude that the velocity of the wave is about 450 m/s. We can say then, from equation (10) and putting $f_{max} (= f_p = 10$ Hz) that the mesh size should be ≤ 5.6 m ($T \leq 1/8.450/10 \Rightarrow T \leq 5.6$ m). Accordingly the mesh used (table 5) meets the conditions required for a dynamic calculation.

4.4. Calculation method

The dynamic simulation was done for four modes, each mode being characterised by the values of ξ_i and f_p ($f_{pmax}=20$ and $f_{pmin}=4$). It will be noted that modes 1 and 2 correspond to dynamic behaviour only after the appearance of the sinkhole, while modes 3 and 4 correspond to dynamic simulation of sinkhole and the excavation. Table 6 shows the parameters used for each mode.

| Simulation | ξ_c | $2\pi \cdot f_p \cdot \xi_c$ | f_p (Hz) |
|------------|---------|------------------------------|--------------------------|
| Mod.1 | 2.5% | 0.628 | 4 (static excavation) |
| Mod.2 | 5% | 1.256 | |
| Mod.3 | 10% | 6.283 | 20 (dynamic excavation) |
| Mod.4 | 20% | 12.566 | |

Table 6: Different models simulated dynamically.

4.5. Analysis of the final configuration

We applied the procedures indicated in paragraph 5. The results for the different modes of dynamic simulation (table 6) concern the shape of the sinkhole “bell” and are given in table 7:

| Simulation | Sinkhole | Shape of bell | | |
|------------|------------|---------------|-----------------------|-------|
| | ϕ (m) | h (m) | α ($^\circ$) | D (m) |
| Mod.1 | 1.4 | 8 | 76 | 7.6 |
| Mod.2 | 1.0 | 8 | 76 | 7.6 |
| Mod.3 | 3.2 | 8 | 82 | 8.2 |
| Mod.4 | 2.4 | 8 | 76 | 7.6 |

Table 7: Shape of the bell and the sinkhole in dynamic mode.

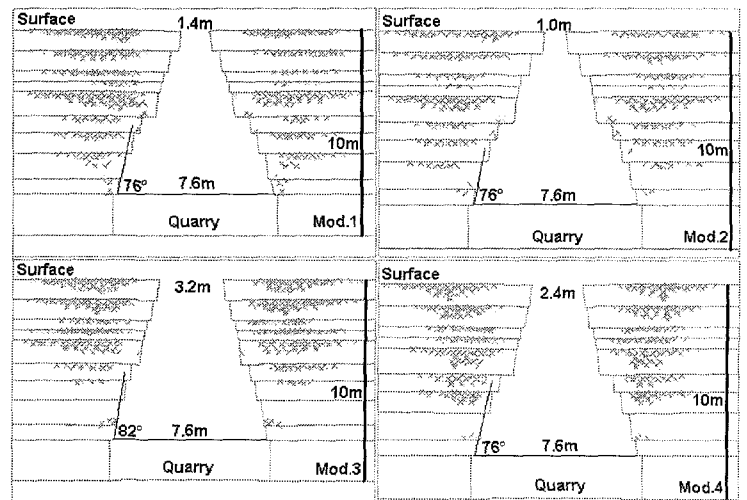


Figure 14: Final dynamic configuration.

Table 7 and figure 14 show the shape of the sinkhole bells together with the relevant parameters. Depending on how the model is simulated dynamically, the diameter of sinkhole at ground level varies between 1.4 and 3.2 m.

The realistic cases (modes 3 and 4) correspond to bigger sinkhole bells than cases (modes 1 and 2). It may be noted that the results (sinkhole bells) as well as the surface movements vary substantially according to the simulation method used (pessimistic or optimistic) and the critical damping value applied.

4.6. Analysis of the final configuration with structure

The configuration of a void with a structure is modelled in dynamic mode (§ 7.5). Table 8 and figure 15 show the results: it can be seen that the sinkhole at the surface has a diameter varying from 2.2 to 3.2 m. The influence of the structure appears in modes 1 and 2 corresponding $f_p=4$ and low critical damping.

| Simulation | Sinkhole | Shape of bell | | |
|------------|------------|---------------|-----------------------|-------|
| | ϕ (m) | h (m) | α ($^\circ$) | D (m) |
| Mod.1 | 2.2 | 8 | 76 | 7.6 |
| Mod.2 | 2.2 | 8 | 76 | 7.6 |
| Mod.3 | 3.2 | 8 | 82 | 8.2 |
| Mod.4 | 2.4 | 8 | 76 | 7.6 |

Table 8: Results in dynamic mode with structure.

The simulation of the model for dynamic excavation (modes 3 and 4), despite the increase in ξ_s , caused considerable perturbation in the roof blocks and very high stresses. The influence of the loads in this type of structure on the block failure processes is negligible. The influence of the structure on the failed spans is also negligible.

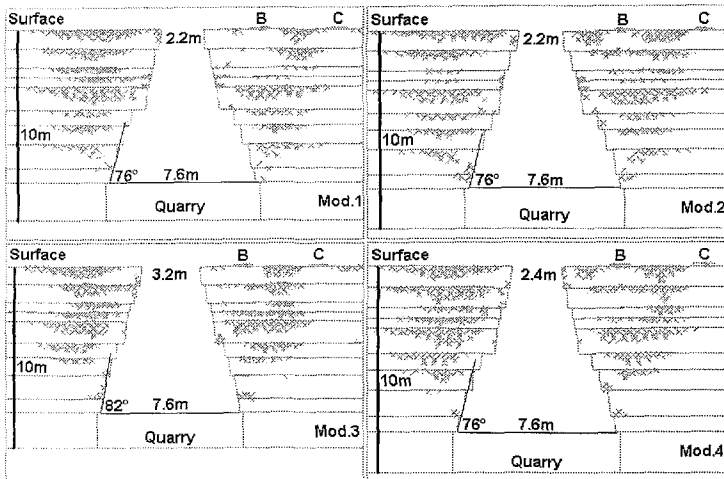


Figure 15: Final configuration in dynamic mode with structure.

5. COMPARISON OF THE SIMULATION RESULTS WITH OBSERVATIONS

We shall refer to the case investigated by Malakoff: this was sinkhole 2.5 m in diameter at the surface and 0.5 m in depth. In order to compare the results obtained with the model and observations, we show table 9 which gives the values obtained for the shape of the bell and sinkhole for all the calculation modes (mean value in dynamic behaviour):

| | Mode | ϕ (m) | Shape of bell | | |
|-------------------|--------------|---------------|---------------|-----------------------|-------|
| | | | h (m) | α ($^\circ$) | D (m) |
| Without structure | Static | 0.0 | 6 | 76 | 7.6 |
| | Dynamic | 2.0 | 8 | 78 | 7.6 |
| With structure | Static | 1.4 | 8 | 76 | 7.6 |
| | Dynamic | 2.5 | 8 | 78 | 7.6 |
| | Observations | 2.5 | 8 | 80 | 7.5 |

Table 9: Results and observations for the profile of the sinkhole.

5.1. Comparison with the calculation in static mode

For static behaviour, and contrary to observation, no sinkhole was observed when no structure was present (table 9). The presence of a structural load led to the formation of sinkhole at the surface, but of smaller diameter (1.4 m rather than 2.5 m). The gap between observation and simulation is narrower. This confirms the influence of external loads on the formation of sinkhole. The values of α ($=76^\circ$) and D ($=7.6$ m) can be used to calculate the maximum geometrical height of the "bell" (h_c) [given by Vachat (1982)]. We have $h_c = D \cdot \tan \alpha / 4$, or 7.6 m. This value is the order of magnitude of those obtained by simulation. The following remarks are relevant: the ingress (or presence) of water, the loads

applied and collapse events at the surface all play a predominant role in the ascent of the "bell" (Vachat, 1982). However, these factors were not modelled.

5.2. Comparison with the dynamic calculation

The results in dynamic mode are closer to observation. The dimensions of the sinkhole are greater. These dimensions are increased further by the combined effects of the structure and the speed of appearance of the sinkhole. The diameter is higher than or equal to that observed in site.

6. INDUCED CONSEQUENCES (OR GROUND-STRUCTURE INTERACTION)

In order to evaluate surface movements and the consequences due to the appearance of sinkhole, it is necessary to introduce the parameters of the subsidence depression (displacement, deformation, gradient, and so on), pointing out that the appearance of sinkhole at the surface causes a change to this depression and, naturally, to these parameters (Al-Heib, 2000). These changes may be limited to the vicinity of the sinkhole diameter (discontinuous movements). Beyond this, the characteristics of the depression and the rate of change of its parameters normally remain unchanged (fig. 16).

Figure 16 shows the half-profiles of vertical displacement (d_y) and horizontal displacement (d_x). It will be seen that the slopes of the vertical and horizontal displacement curves in dynamic mode are greater than those in static mode.

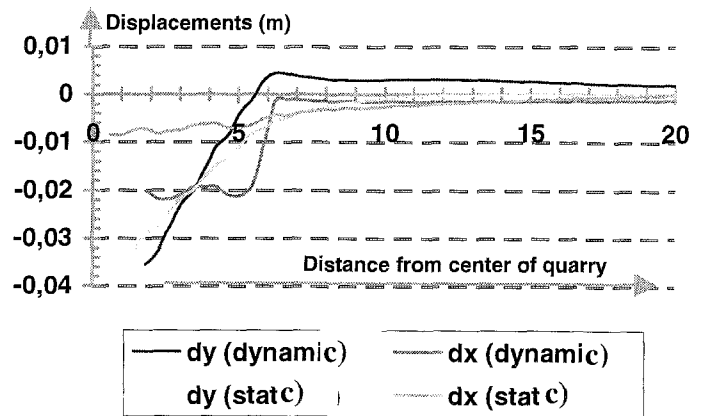


Figure 16: Variations in the half-profiles of displacements.

Table 10 shows the displacements and deformations at the locations of the foundations A, B and C: It can be seen that:

- ✓ the dynamic calculation causes heave at foundation (C), apparently due to substantial collapse of the ground after appearance of the sinkhole;
- ✓ the maximum values induced at foundation C are due to the static calculation;
- ✓ the deformation induced at the foundations is practically negligible. This is confirmed in practice (rigid foundations prevent or minimise the deformation of the ground, see Deck 2002).

| Foundations | A | B | C |
|----------------------|----------|--------------|-----------------------------|
| d_y (mm) | Sinkhole | -16.0 (stat) | -2.60 (stat) +3.10 (dyn) |
| d_x (mm) | Sinkhole | -19.3 (dyn) | -3.2 (stat) |
| ε (mm/m) | Sinkhole | +0.3 (stat) | +0.4 (stat) -0.2 (dyn) |
| G (mm/m) | Sinkhole | +11.8 (dyn) | +1.5 (stat) -0.5 (dyn) |

Table 10: Parameters for deformations induced by the sinkhole.

These remarks suggest that the dynamic behaviour induces more substantial consequences.

In table 10 the term sinkhole indicates that sinkhole has completely damaged foundation (A). Its stability could be assured by appropriate methods (Al-Heib, 2000), for example:

- ✓ filling the underground cavity by injection;
- ✓ building a special foundation to prevent this occurrence (fig. 17a);
- ✓ building the structure over an overall raft (fig. 17-b) or with a gantry structure (fig. 17-c) to resist the collapse of the ground under the foundation.

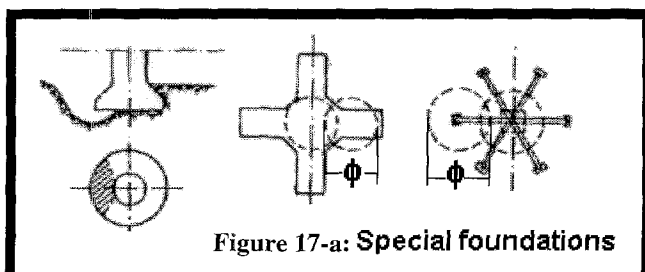


Figure 17-a: Special foundations

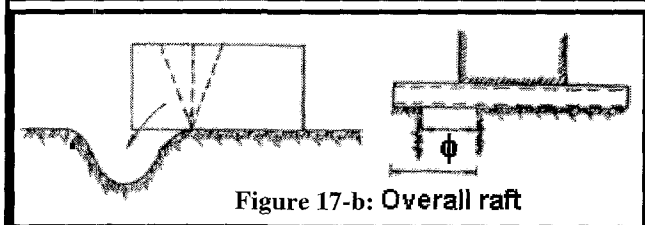


Figure 17-b: Overall raft

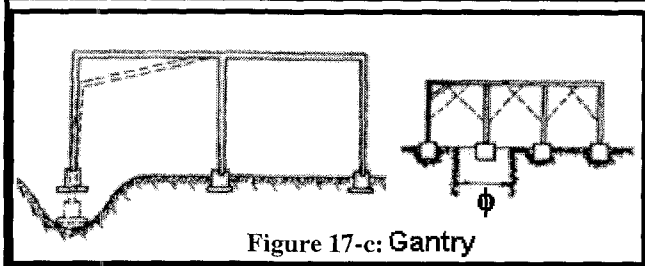


Figure 17-c: Gantry

Figure 17: Some measures of protection against sinkhole (Tolmatshev et al 1990).

As far as foundations B and C are concerned, their size will accommodate the relevant movements.

7. CONCLUSIONS AND OUTLOOK

The study was able to:

- ✓ simulate and provide understanding of the phenomenon of the ascent of the “bell” as a result of the manual creation of induced fractures;
- ✓ predict the form of the propagation of the sinkhole towards the surface;
- ✓ show that the presence of a structure at the surface can accelerate the movement of the void towards the surface (aggravating factor);
- ✓ confirm that the sudden failure of roof blocks applied in the dynamic calculation generates resonance forces that enhance the growth of the underground void;
- ✓ predict the shape of the settlement depression and deduce the movements induced in the affected structures.

The calculation procedures used represent a novel method for predicting the appearance of sinkhole and for evaluating its induced consequences in affected structures. This modelling approach could not be generalised unless applied to several cases. The aim is therefore to extend this methodology so as also to encompass parameters related to the environment (ground, structures, and so on).

8. BIBLIOGRAPHY

Al-Heib 2000 : « Effets et conséquences des mouvements du sous-sol sur le bâti. Synthèse des principales méthodes de prévention et de protection ». Ref INERIS-DRS-00-25315RN01.

Bart 2000 : « Contributions à la modélisation du comportement hydromécanique des massifs rocheux avec fractures. ». Thesis of the university of sciences and technologies of Lille; Laboratory of mechanics of Lille U.R.A 1441 C.N.R.S. Pp. 14-37.

Cundall 1980 : « A generalized Distinct Element » : Program for modelling jointed rock, UDEC, ITASCA. Consulting Group Inc. Minneapolis U.S.

Deck 2002 : « Estimation de la vulnérabilité d'une structure soumise à un affaissement minier ». Conference AUGC, Toulouse, France 2002.

Didier et Tritsch, 1996 : « Traitement des carrières souterraines abandonnées par remblayage partiel ». INERIS, ref : SSE-JTr-Cdi/CS 24EA05/R01.

El-shabrawy 1996 : « Comportement des ouvrages historiques soumis à des sollicitations sismiques ». Thesis INPL, LAEGO, EMN ; supported the 25 oct. 1996.

Filliat 1981 : « La pratique des sols et fondations ». Monitor Ed., 1984. Pp. 319-355 and pp. 1315-1351.

Fine 1993 : « Le soutènement des galeries minières ». Pp.27-42. Editor : ARMINES : Center of geotechnics and exploitation of the underground. 35 rue saint Honoré, 77305 Fontainebleau.

Herget 1988 : « Stresses in rock ». « A.A.Balkema, Rotterdam 1988 » : ISBN 90 6191 685 2. Pp. 136-146.

Itasca 1996 : « Consulting group ; Inc (1996), UDEC (universal Distinct Element Code). Version 3, Volume I et II.

Mandel 1966 : « Cours de mécanique des milieux continus ». Mécanique des solides, tome II. Paris Ed. :Gauthier-Villars editor, 1966. Pp. 497-505.

Pecker 1984 : « Dynamique des sols » : Press National School of the Bridges and Chaussées. ISBN 2-85978-072-6.

Peng et Cheng 1981 : « Predicting surface sinkhole for damage prevention ». Coal Min Process, V18, N5, May 1981. Pp. 84-95.

Piguet 1983 : « La modélisation en mécanique des terrains et son application à l'exploitation minière ». Thesis INPL supported le 29 avril 1983.

Prévost et Hoëg 1975 : Cited by Philippe MESTAT 1993 : « Lois de comportement des géomatériaux et modélisation par la méthode des éléments finis » Pages 104-105.

Tharp 1995 : « Design against collapse of karst caverns ». « Karst geohazards », Beck ed., 1995 Balkema, Rotterdam, ISBN 90 5410 535 6.

Tolmatshev, Reuter et V.V. 1990 : Bauen und bergbau in senkungsund erdfallgebieten. Eine Ingenieurgeologie des karstes : « Schriftreihe Geologische Wissenschaften, V. 28, Akademie-Verlag, Berlin (in German).

Vachat 1982 : « Les désordres survenant dans les carrières de la région parisienne ». Report diploma Engineer CNAM, Paris, 1982.

9. ACKNOWLEDGEMENT

Some of the work described formed part of the research program of the department of ground and underground hazards of INERIS (ETAT-DRS-02) funded by the French Ministry for Land-Use Planning and the Environment (MATE), "Analysis, prevention and control of ground movement risks arising from the presence of underground voids". We should like to express our gratitude to MATE which enabled this research to be carried out.